

# A COMPARISON BETWEEN CYCLE-GAN BASED FEATURE TRANSLATION AND OPTICAL-SAR VEGETATION INDICES

E. Çolak<sup>1\*</sup>, F. Sunar<sup>2</sup>

<sup>1</sup> Chemnitz University of Technology, Chemnitz, Germany emre.colak@etit.tu-chemnitz.de

<sup>2</sup> ITU, Civil Engineering Faculty, Geomatics Engineering Department, 80626 Maslak Istanbul, Turkey fsunar@itu.edu.tr

Commission III, WG III/7

**KEY WORDS:** Cycle-GAN, Deep Learning, Vegetation Indices, Feature Translation, Change Detection.

## ABSTRACT:

Optical and microwave remote sensing technologies have become key tools for local and global change detection applications. Generally, optical data has been the focus of remote sensing for change detection because of the varied spatial and temporal resolutions that allow for reliable information. However, the dependence of optical data on weather conditions prevents continuous and up-to-date information. On the other hand, Synthetic Aperture Radar (SAR) data can record all-weather and all-time polarization information which is critical for change detection in poor weather conditions; nonetheless, SAR is not precise as optical data for forestry change detection applications as it cannot provide the spectral features of interest. The combined processing of optical and SAR images allow for the retrieval of information of interest with a precision that none of them could achieve alone. In this context, Cycle-Consistent Generative Adversarial Networks (CycleGAN) based deep feature translation method was proposed in this study for change detection. The CycleGAN transfers images from one domain (optical) to another domain (SAR) into the same feature space using a cyclic structure. Thus, it can provide continuous and up-to-date information for change detection while keeping its spectral features. The accuracy of the fake images generated from CycleGAN was evaluated by correlating them with spectral indices (e.g., Normalized Difference Vegetation Index (NDVI), Modified Radar Vegetation Index (mRVI), and Modified Radar Forest Degradation Index (mRFDI)) directly obtained from optical and SAR data. As a result, the best correlation coefficients (R) were found between real NDVI (optical data) and fake NDVI (CycleGAN) with 0.98 and 0.97 for two different dated datasets.

## 1. INTRODUCTION

The optical remote sensing data has received the most attention for change detection applications. Optical data with varying spatial and temporal resolutions can not only convey spectral information about earth features, but also reflect their texture and geometric shape, ensuring that change detection is accurate. Some spectral indices produced by mathematical combination or transformation of spectral bands have been found to be quite useful for detecting changes, for example the Normalized Difference Vegetation Index (NDVI), which is used especially in forest areas.

Synthetic aperture radar (SAR) data, on the other hand, reflect the scattered information of the ground surface in any weather condition and at any time. Thus, SAR images have an advantage for specific change detection applications due to their independence from lighting conditions. Vegetation indices (e.g. Modified Radar Vegetation Index (mRVI) and Modified Radar Forest Degradation Index (mRFDI)) similar to NDVI produced from SAR data, as in optical data, can be used quite successfully in changing forest areas.

However, it is not always easy to get results as precise as NDVI from vegetation spectral indices produced by SAR. Since optical remote sensing data provides crucial spectral information in monitoring the phenological stages of forests, optical-based spectral indices can provide much precise information in forestry. In spite of its capabilities, a continuous time series of optical remote sensing data is difficult to gather due to the weather dependence of optical image acquisitions, and the data only

offers information on the top layer of vegetation. SAR images are a reliable alternative to the limitations of optical images as mentioned before. Unlike optical reflectance, backscattering coefficients are affected by characteristics of the target such as roughness, moisture, biomass, vegetation structure, and height. Hence, the simultaneous processing of optical and radar temporal sequences allows for the retrieval of information of interest with a precision that none of them could achieve alone (Wang et al., 2019; Li et al., 2021; Şener et al., 2021).

In recent years, deep learning algorithms for feature translation have been used in remote sensing in order to benefit from the information of both optical data and radar data. A deep learning (DL) based method namely Cycle-Consistent Generative Adversarial Networks (Cycle-GAN), uses a cyclic architecture to transfer images from one domain (optical) to another domain (SAR) into the same feature space (Wang et al., 2019; Li et al., 2021; Şener et al., 2021).

The main purpose of this study is to perform a feature translation between Sentinel-1 SAR and Sentinel-2 optical data based on Cycle-GAN, when there is a missing specific feature in cloudy weathers. Furthermore, the Cycle-GAN based data is compared with other classical optical-SAR-based spectral indices NDVI, mRVI, and mRFDI.

## 2. STUDY AREA

As a study area, Sinop Nuclear Power Plant area is selected. This area is detailed discussed in (Çolak et al., 2019) and (Çolak et al., 2021). The Sinop Nuclear Power Plant was a planned nuclear

power plant area in Turkey's far north, in the Sinop Peninsula, where 99% of the land is covered in forest (Figure 1). It is estimated that around 650000 trees have been felled in order to construct the nuclear power station (Çolak et al., 2019, 2021). In addition, for 2018, opponents of the project stated in local news that 130 hectares of forest area were deforested and a total of 225 thousand trees were cut (CnnTurk, 2014).

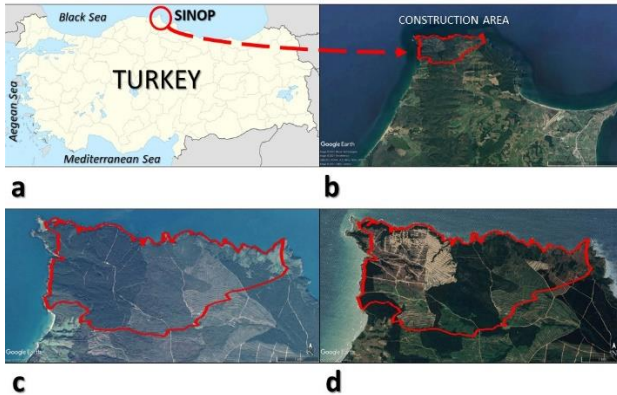


**Figure 1.** The map of (a) Turkey, and satellite images of (b) construction area of Sinop nuclear power plant, (c) construction area in 2016, and (d) construction area in 2019 (©Google Earth).

### 3. DATA COLLECTION

In the analysis, Sentinel-1 and Sentinel-2 were used as data sets and their properties are given in Table 1.

Mission	Sensors	Temporal resolution (day)	Spatial resolution (m)
Sentinel 1	C - Band SAR	12	(SM) & (IW) 10 x 10, (EW) 25 x 25
Sentinel 2	Multispectral Instrument (MSI)	10	10, 20 & 60

**Table 1.** The characteristics of Sentinel-1 and -2 data (Soille et al., 2016).

The feature translation based on Cycle-GAN was carried out by determining the most appropriate data set between the start date of the construction of the nuclear power plant (April 2017) and the date when the construction was temporarily stopped (July 2019). The most appropriate dataset was chosen with attention to whether the Sentinel-2 data was successively completely cloudless. Accordingly, as can be seen in the Figure 2, two different time periods (i.e. March - May 2017 and June - August 2019) for Sentinel-2 data were examined. More specifically, the most appropriate dates were chosen as 28 and 29 March for Sentinel-2 and -1, respectively before logging, 28 and 29 June 2019 for Sentinel-2 and -1, respectively after logging.

### 4. METHODOLOGY

Various image-processing steps and analysis such as pre-processing, vegetation indices, deep feature translation, statistical analysis, and change detection were applied. First, NDVI results were compared statistically; and then two methods used to detect

changes in vegetation areas were compared and evaluated (Figure 3).

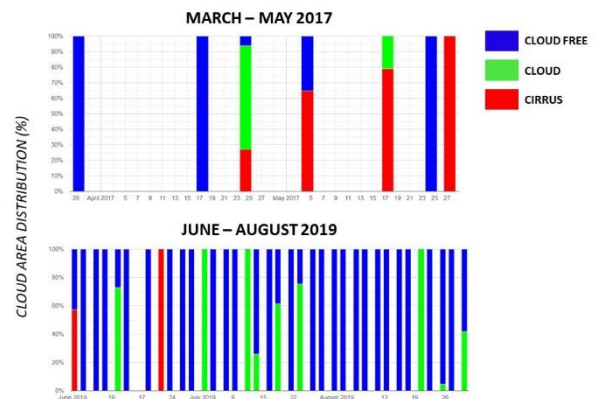


**Figure 2.** Cloudiness of available Sentinel 2 data over two different time scales in Sinop Nuclear Power Plant Construction Area.

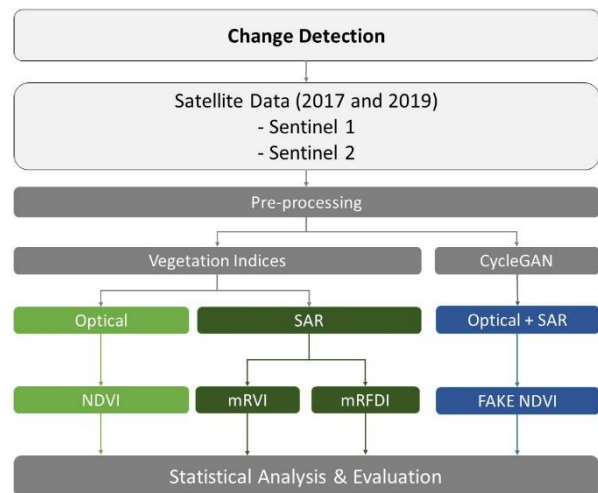


**Figure 3.** Flowchart of the study.

#### 4.1 Vegetation Indices

The highly known NDVI, which varies between -1 to 1, is often used to characterize annual changes in forest areas and state the vegetation phenology. Besides the optical data, SAR based vegetation indices Modified Radar Vegetation Index (mRVI) and Modified Radar Forest Degradation Index (mRFDI) are very useful in forestry observations as they take into account the key parameters like biomass, structure, and moisture (Flores et al., 2019; Çolak et al., 2019, 2021) (Table 2).

#### 4.2 Cycle-Consistent Generative Adversarial Networks (Cycle-GAN)

As classic models of probability generation, Generative Adversarial Networks (GANs) can figure out the internal data distribution by learning a large amount of data. GANs generate data in an unsupervised deep learning method for image generation. In other words, GANs are models that use two networks — a generator and a discriminator — to generate new images. The Cycle-GAN, a GAN model, was created with a cycle constraints framework for image-to-image translations (Şener et al., 2021).

Index	Formula & Interpretation	Application
NDVI	$NDVI = \frac{NIR - Red}{NIR + Red}$ <p>Range (-1 - +1): Negative values indicates most probably water body. Values close to +1 indicates dense green vegetation. Values close to zero indicate low vegetation cover.</p>	Monitoring vegetation phenology. It assess direct effects of climatic conditions on biomass and phenological patterns of vegetation.
mRVI	$mRVI = \left( \frac{\gamma_{VV}^0}{\gamma_{VV}^0 + \gamma_{HH}^0} \right)^{0.5} \left( \frac{4\gamma_{VH}^0}{\gamma_{VV}^0 + \gamma_{HH}^0} \right)$ <p>Range (0 - 1): Low values refer low vegetation cover and water content. The low threshold can be used to separate forest and non-forest.</p>	Monitoring vegetation cover, water content, and aboveground biomass with quad-pol or quasi-quad-pol data.
mRFDI	$mRFDI = \frac{\gamma_{VV}^0 - \gamma_{VH}^0}{\gamma_{VV}^0 + \gamma_{VH}^0}$ <p>Range (0 - 1): Low values refer to high biomass and intact forests. Values change gradually to higher values for degraded and non-forest areas. The values remain independent of topography.</p>	Detecting forest degradation and deforestation, biomass loss and gain with dual-pol or quad-pol data.
<p>NIR: Near Infrared band, Red: Red band.  <math>\gamma^0</math>: Radiometrically and geometrically corrected SAR backscattering coefficient for each polarization combination in linear units (<math>m^2/m^2</math>).</p>		

**Table 2.** Optical - SAR vegetation indices (Flores et al., 2019; Tucker, 1979).

Cycle-GANs were proven to improve performance mainly in areas such as crop type mapping and identification, change detection, and wildfire detection (Liu and Lei, 2018; Soto et al., 2020; Şener et al., 2021; Li et al., 2021; Park et al., 2020).

A Cycle-GAN is mathematically defined by Eq.1 below.

$$L(F, G, D_X, D_Y) = L_{GAN}(F, D_Y) + L_{GAN}(G, D_X) + \lambda L_C(F, G) \quad (1)$$

Where  $L_{GAN}(G, D)$  denotes the classical GAN loss function involving a generator  $G$  and a discriminator  $D$ , whereas  $L_C(F, G)$  stands for the cycle loss which is given by Eq.2 below.

$$L_C(F, G) = E_{x \sim X} [\|G(F(X)) - x\|_1] + E_{y \sim Y} [\|F(G(Y)) - y\|_1] \quad (2)$$

and  $\lambda$  is a hyper-parameter (Wang et al., 2019).

The purpose of Cycle-GAN image-to-image translation is to learn the mapping between an input image and an output image using a training set of aligned image pairs, which is a class of vision and graphics challenges (Zhu et al., 2017).

One of the most significant advances made possible by GANs in the image-to-image translation challenge is the learning of a structured loss that penalizes the overall configuration of the output rather than one in which each output pixel is treated independently of the rest in the input image (Ren et al., 2020).

Without depending on paired images, CycleGAN is a technique for image-to-image translation from the reference image domain (X) to the target image domain (Y) (Park et al., 2020; Ren et al. 2020). Where X and Y are optical (i.e. NDVI band calculated from Sentinel-2 NIR and Red bands as a feature) and radar (i.e. Sentinel-1's VV (vertical transmit and vertical receive polarisation) and VH (vertical transmit and horizontal receive polarisation) polarised bands as features) domains, respectively in this study.

Figure 4 shows the basic structure of the CycleGAN used.

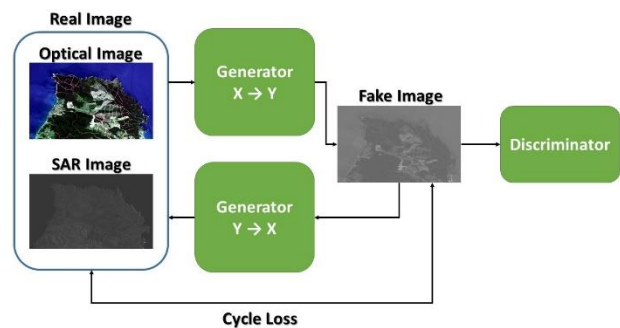


**Figure 4.** The basic structure of CycleGAN.

In this study, the images were split to small patches to create image pairs. While 100 image pairs were created for training, 25 image pairs were created for the test. The scarcity of data used is due to the small study area (10.1 square kilometres).

### 4.3 Statistical Analysis & Evaluation

Correlation analysis is the simplest way for examining the relationship between two variables. The Pearson's correlation coefficient, abbreviated R, is a fundamental statistical approach for quantifying the degree of relation between linearly related variables in remote sensing applications. It is determined by dividing the covariance of the two variables by the product of their standard deviations (Chen et al., 2018).

In the statistical analysis, the Pearson's correlation coefficient method was performed between the CycleGAN output fake image and optical – SAR vegetation indices.

For evaluating the results, difference maps were generated, and all results were given spatially and quantitatively.

## 5. RESULTS

### 5.1. Vegetation Indices

Firstly, the vegetation indices NDVI, mRVI, and mRFDI were generated from Sentinel -2 and -1 data for both 2017 and 2019 datasets (Figure 5).

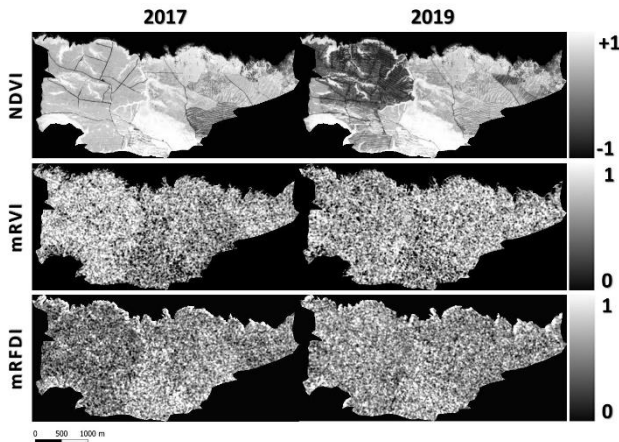


**Figure 5.** Vegetation indices for both 2017 and 2019 datasets.

As can be seen in Figure 5, the difference in the 2017 and 2019 NDVI images is clearly visible. However, the change in mRVI and mRFDI indexes produced from SAR data is not clearly visible as in NDVI, but a difference can still be observed. Hence, these results support that these indices are not as precise as NDVI.

### 5.2. Cycle-GAN

As mentioned before, the images were split to small patches to create image pairs for applying the Cycle-GAN (Figure 6).

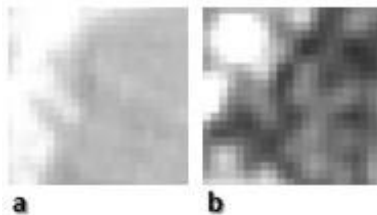


**Figure 6.** A sample image pair used for training and test (a) NDVI (Optical) (b) SAR.

Consequently, CycleGAN was applied to specified datasets by the indicated feature inputs (Figure 7).

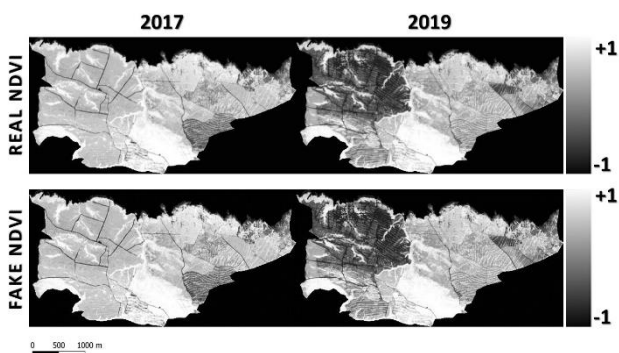


**Figure 7.** NDVI and image-to-image translated fake NDVI using Cycle-GAN.

As seen in Figure 7, Cycle-GAN gave very successful results. Spatially, there is almost no difference between real NDVI and fake NDVI.

### 5.3. Statistical Analysis & Evaluation

As showed in Table 3, to evaluate the strength of the relation, a correlation study between the real-fake NDVI and radar vegetation indices was conducted using the Pearson correlation coefficient.

Correlation Analysis	Before logging (2017)	After logging (2019)
NDVI – Fake NDVI	0.98	0.97
NDVI - mRVI	0.39	0.35
NDVI - mRFDI	0.40	0.31
Fake NDVI - mRVI	0.51	0.43
Fake NDVI - mRFDI	0.53	0.41

**Table 3.** The Pearson's correlation coefficient (R) between the vegetation indices.

As a result, a very high correlation (0.98 and 0.97 between 2017 and 2019 datasets, respectively) was observed between real NDVI and fake NDVI. Thus, it has been shown how successful the fake NDVI produced with Cycle-GAN is both spatially and quantitatively. On the other hand, no high correlation was observed between real - fake NDVI and radar vegetation indices.

Furthermore, difference maps between 2017 and 2019 dataset were produced to evaluate the vegetation indices produced in terms of change detection (Figure 8).

As can be seen from Figure 8, real and fake NDVI gave almost similar results spatially, whereas radar vegetation indices did not.

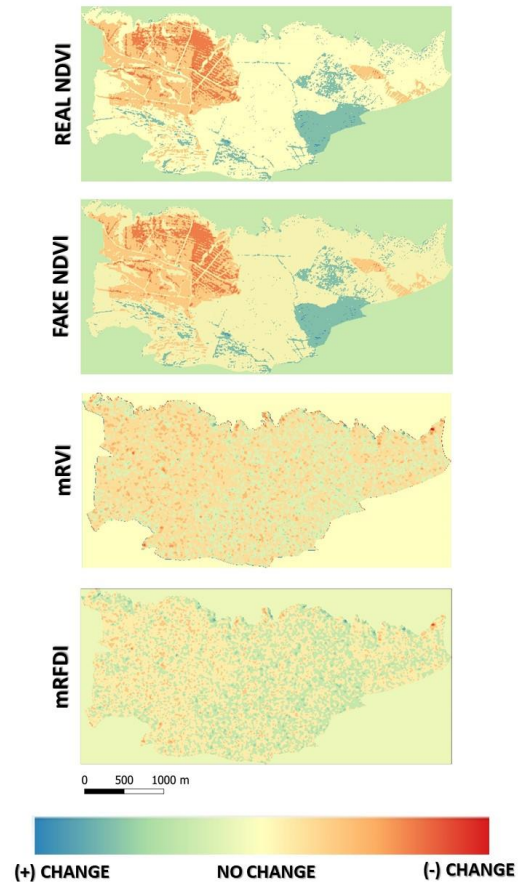


**Figure 8.** Difference maps for all vegetation indices and Cycle-GAN based fake NDVI.

In particular, the cut forest area was calculated in both maps to quantitatively evaluate the similarity of the real NDVI and fake NDVI results (Table 4). As a result, very similar results were obtained here as well. While the cut forest area with real NDVI was calculated as 248.2 ha, this area was calculated as 247.9 ha with fake NDVI.

Vegetation Indices	Areal extent of cut forest area (ha)
Real NDVI	248.2
Fake NDVI	247.9

**Table 4.** Difference maps in cut forest area (ha) for real and fake NDVI.

Considering that there is one tree in 10 square meters with the most optimistic calculation, this means that approximately 250 thousand trees have been cut, which is very close to the amount of tree cut (225 thousand) stated in the local news.

## 6. CONCLUSION

Because of the diverse spatial and temporal resolutions that provide for accurate information, optical data has been the main source of remote sensing for change detection. The dependence of optical data on weather conditions, on the other hand, intercept continuous and up-to-date data. Although SAR data compensates for this deficiency, it cannot provide a complete solution because of its lack for spectral features of interest.

As shown in this study, deep learning techniques can be used to benefit from the information (spectral feature, roughness, moisture, biomass, vegetation structure, and height etc.) provided by both data (optical and SAR), as well as to provide continuous and up-to-date information. Cycle-GAN, a deep learning based method, uses a cyclic structure to translate the image from optical domain to the target SAR domain. As demonstrated, the fake NDVI generated with Cycle-GAN gave very successful results both spatially and quantitatively.

As a result of the correlation analysis, the relationship between real NDVI and fake NDVI was obtained as 98% and 97% for the 2017 and 2019 datasets, respectively, and was considered quite successful. In addition, a difference map between 2017 and 2019 was produced with both real NDVI and fake NDVI. Consequently, the areal extent of cut forest areas determined by real NDVI and fake NDVI were found to be 99.9% similar (i.e. 248.2 ha and 247.9 ha, respectively).

Finally, it is seen that machine or deep learning techniques give a great impetus to classical image processing techniques and provide a new alternative to optical-SAR data fusion. In particular, these techniques facilitate the use of increasing data diversity (multi-sensor) and redundancy (big data). In future studies, the performance of deep learning techniques will also be evaluated temporally, using time-series data from the Google Earth Engine (GEE) platform.

## REFERENCES

Chen, W., Zhang, S., Li, R., Shahabi, H. 2018. Performance evaluation of the GIS-based data mining techniques of best-first decision tree, random forest, and naïve Bayes tree for landslide

susceptibility modeling. *Science of The Total Environment* (644), 1006-1018. <https://doi.org/10.1016/j.scitotenv.2018.06.389>.

CnnTurk, 2014. Sinop'ta nükleer santral için ağaç katliamı [Tree massacre for nuclear power plant in Sinop] <https://www.cnntrk.com/haber/turkiye/sinopta-nukleer-santral-icin-agac-katliami>.

Çolak, E., Chandra, M., Sunar, F. 2019. The Use of Multi-Temporal Sentinel Satellites in the Analysis of Land Cover/Land Use Changes Caused By the Nuclear Power Plant Construction. *Int. Arch. Photogramm. Remote Sens. Spatial Inf. Sci.*, Xlii-3/W8, 491–495, <https://doi.org/10.5194/isprs-archives-Xlii-3-W8-491-2019>.

Çolak, E., Chandra, M., Sunar, F. 2021. The Use of Sentinel 1/2 Vegetation Indexes with GEE Time Series Data in Detecting Land Cover Changes in the Sinop Nuclear Power Plant Construction Site. *The International Archives of Photogrammetry, Remote Sensing and Spatial Information Sciences*, 43, 701-706.

Flores, A., Herndon, K., Thapa, R., Cherrington, B. 2019. The SAR Handbook: Comprehensive Methodologies for Forest Monitoring and Biomass Estimation, doi.: 10.25966/nr2c-s697.

Li, X., Du, Z., Huang, Y., Tan, Z. 2021. A deep translation (GAN) based change detection network for optical and SAR remote sensing images. *ISPRS Journal of Photogrammetry and Remote Sensing*, 179, 14-34.

Liu, L., Lei, B. 2018. Can SAR images and optical images transfer with each other?. In *IGARSS 2018-2018 IEEE International Geoscience and Remote Sensing Symposium* (pp. 7019-7022).

Ren, C.X., Ziemann, A., Theiler, J., Durieux, A.M. 2020. Cycle-consistent adversarial networks for realistic pervasive change generation in remote sensing imagery. In *2020 IEEE Southwest Symposium on Image Analysis and Interpretation (SSIAI)* (pp. 42-45).

Park, M., Tran, D.Q., Jung, D., Park, S. 2020. Wildfire-Detection Method Using DenseNet and CycleGAN Data Augmentation-Based Remote Camera Imagery. *Remote Sensing*, 12(22), 3715.

Soille, P., Burger, A., Rodriguez, D., Syrris, V., Vasilev, V. 2016. March. Towards a JRC earth observation data and processing platform. In *Proceedings of the Conference on Big Data from Space (BiDS'16)*, Santa Cruz de Tenerife (pp. 15-17).

Soto, P.J., Costa, G.A.O.P., Feitosa, R.Q., Happ, P.N., Ortega, M.X., Noa, J., Almeida, C.A., Heipke, C. 2020. Domain Adaptation With CycleGAN For Change Detection In The Amazon Forest. *Int. Arch. Photogramm. Remote Sens. Spatial Inf. Sci.*, XLIII-B3-2020, 1635–1643, <https://doi.org/10.5194/isprs-archives-XLIII-B3-2020-1635-2020>.

Şener, E., Çolak, E., Erten, E., Taşkın, G. 2021. The Added Value of Cycle-GAN for Agriculture Studies. In *2021 IEEE International Geoscience and Remote Sensing Symposium IGARSS* (pp. 7039-7042).

Tucker, C.J. 1979. Red and photographic infrared linear combinations for monitoring vegetation. *Remote sensing of Environment*, 8(2), 127-150.

Wang, L., Xu, X., Yu, Y., Yang, R., Gui, R., Xu, Z., Pu, F. 2019. SAR-to-optical image translation using supervised cycle-consistent adversarial networks. *IEEE Access*, Vol.7, pp.129136-129149.

Zhu, J.Y., Park, T., Isola, P., Efros, A.A. 2017. Unpaired image-to-image translation using cycle-consistent adversarial networks. In Proceedings of the IEEE international conference on computer vision (pp. 2223-2232).